Supporting Information: Effect of Surface Ligands on Gold Nanocatalysts for CO_2 Reduction

Hongyu Shang,[†] Spencer K. Wallentine,[†] Daniel M. Hofmann,[‡] Quansong Zhu,[¶] Catherine Murphy,[‡] and L. Robert Baker*[,†]

†*Department of Chemistry and Biochemistry, The Ohio State University, Columbus, OH 43210*

‡*Department of Chemistry, University Illinois at Urbana-Champaign, 600 South Mathews Avenue, Urbana, IL 61801*

¶*Department of Chemistry and Biochemistry, The Ohio State University, 100 West 18th Avenue, Columbus, OH 43210*

E-mail: baker.2364@osu.edu

Phone: +1 (614) - 292 - 2088

Contents

1. Experimental details

Sample preparation

Gold nanoparticle synthesis, characterization, and electrode preparation

Au nanoparticles were synthesized using a modified Brust method that has been reported previously.[1–3] A summary of the particle size distributions is given in Table S1.

Table S1: A summary of the size distributions for different samples

Sample	Size Distribution (nm)
DDT-Au	2.1 ± 0.4
UVO-Au	Not discrete particles
PPh_3-Au	2.0 ± 0.7
DDT-CuAu	2.0 ± 0.5[1]

Au nanoparticles we characterized using high-angle annular dark-field scanning transmission electron microscopy (HAADF-STEM), as shown in Figure S1.

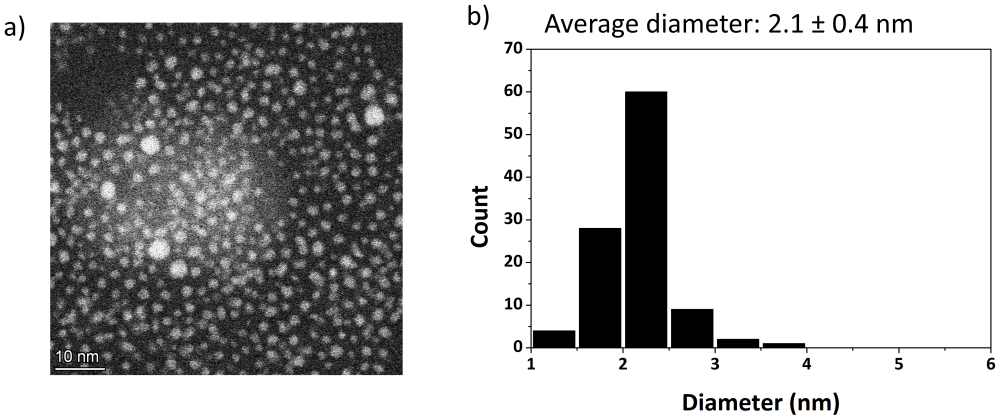

Figure S1: (a) HAADF-STEM images and (b) histogram of DDT-Au nanoparticles

UVO-Au was prepared by removing the capping agent using a custom built UV ozone cleaning box.[4] Samples were treated for 1 h and subsequently washed with millipore water. Two parallel low-pressure Hg lamps (Light Sources Inc., model GPH357T5VH/4P) with a distance of 2.5 cm were used as the UV source. The sample was at a fixed height of 1.2 cm

under the two lamps. Figure S2 (a/c) and (b/d) show the dodecanethiol Au 4f / S 2p XPS before and after the removal procedure, respectively. An obvious S peak is observed for the DDT-Au sample before UV/ozone cleaning, which is completely removed following cleaning for 1 h.

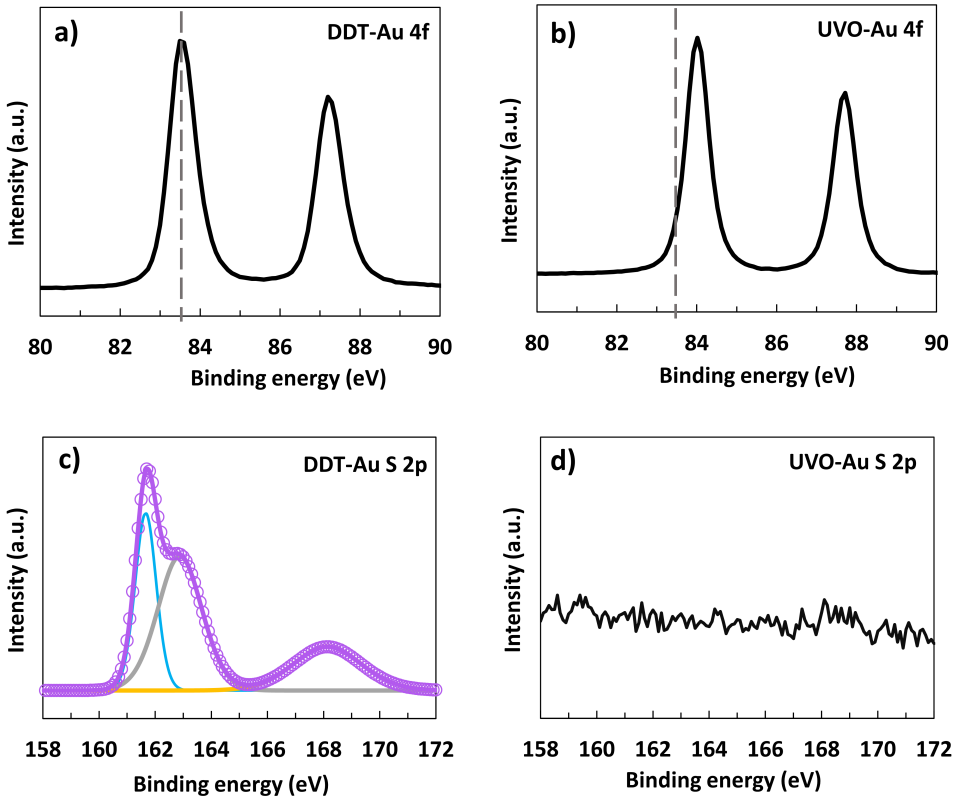

Figure S2: XPS spectra of Au 4f for a) DDT-Au and b) UVO-Au. The dashed line indicates a blue shift of 0.5 eV of Au 4f for UVO-Au. XPS spectra of S 2p for c) DDT-Au and d) UVO-Au.

To understand the effects of removing the capping agent on the nanoparticle morpholgoy, we also took TEM images of the nanoparticles drop cast onto a 50 nm silicon nitride membrane. After removal of the capping agent the particles sinter together to form a network structure as shown in Figure S3.

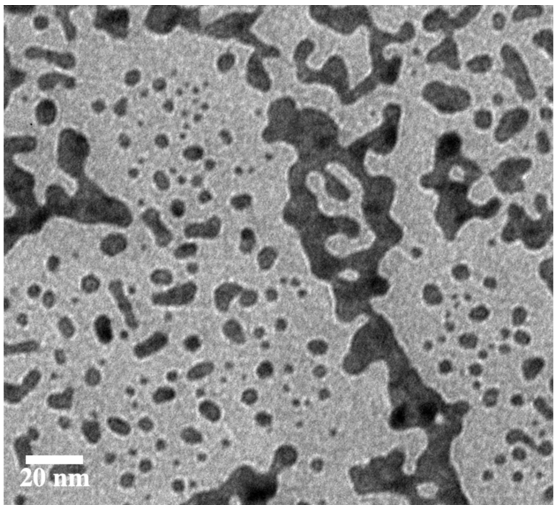

Figure S3: Post UV ozone treated nanoparticles imaged by TEM.

Triphenylphosphine nanoparticles (PPh_3-Au) were as reported previously, except the dodecanethiol capping agent was replaced by an equivalent amount of triphenylphosphine.[1] Figure S4 (a) and S4 (b) show transmission microscopy of PPh_3-Au, and the associated size distribution which shows that the nanoparticles are 2.0 ± 0.7 nm.

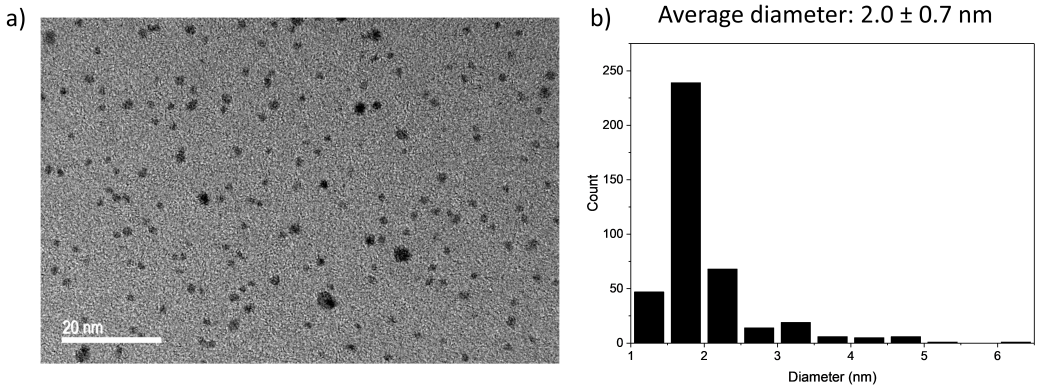

Figure S4: (a) TEM characterization and (b) histogram of PPh_3-Au nanoparticles

Glassy carbon (Alfa Aesar) was used as the working electrode substrate, and was polished with 50 nm alumina, thoroughly washed with Milli-Q water, and dried with nitrogen prior to nanoparticle loading. The working electrode was prepared by drop-casting 75 μl of 50 μM nanoparticle solution on the substrate. The mass loading for each sample is about 250 μg without considering the mass of DDT. Then the electrode was dried in the air for one hour

to evaporate the solvent.

Polycrystalline gold working electrode preparation

PC-Au electrodes were prepared to provide a comparison to DDT-Au. Before Au deposition, the glass substrates were cleaned using basic Piranha (H_2O:H_2O_2:NH_4OH 5:1:1. Caution: Pirhana solutions are caustic and should be handled with extreme care) at 80 °C for one hour. PC-Au electrodes were prepared by electron beam evaporation on a Kurt J. Lesker Lab-18 system. First, a 20 nm chromium adhesion layer was deposited, followed by 100 nm of Au. The deposition rates were 0.9 $\AA$/s and 1.3 $\AA$/s for Cr and Au, respectively, as measured by quartz crystal microbalance. Before each chronoamperometry experiment the PC-Au electrode was cleaned in basic piranha for 5 min and washed thoroughly with Milli-Q water. To prepare 1-dodecanethiol self-assembled monolayers on PC-Au, the Au substrate was prepared by soaking basic piranha cleaned PC-Au in a 20 μM ethanoic solution of 1-dodecanethiol overnight. Before use, the sample was rinsed with ethanol several times to remove any unbound thiol on the surface and finally dried with nitrogen.[5]

Electrochemical measurements

Electrochemical measurements were made using a BioLogic SP-50 potentiostat. A custom batchmode headspace sampling system was used to measure the gas phase products during CO_2R by connecting an Agilent 7890B gas chromatograph to a custom two compartment glass H-cell. A MoleSieve column was used to separate gas products. A thermal conductivity detector was used to detect hydrogen and a nickel catalyst and flame ionization detector were used to detect carbon species. During CO_2R, the headspace is filled with CO_2 (Praxair, 99.9%) at atmospheric pressure. A nafion membrane, which was activated in 10% H_2SO_4 at 100 °C for 10 min before every experiment and stored in Milli-Q water after use, was used to separate the two compartments of the H-cell. Pt was used as the counter electrode (CE) and Ag/AgCl (LowProfile Silver/Silver Chloride Gel Reference Electrode (74 mm long),

PINE) was used as the reference electrode (RE). 0.1 M sodium bicarbonate (Sigma-Aldrich, $\geq$ 99.5%) in milli-Q water (18.2 ohm) was used as the electrolyte. Prior to each experiment, high purity CO_2 was purged towards the working electrode (WE) until the pH reached 6.8. 3.4 μM EDTA (Ethylenediaminetetraacetic acid) was added to the 0.1 M sodium bicarbonate solution to remove any metal ion contamination in the electrolyte for the indicated experiments.[6] After each experiment, the H-cell was soaked in 40% sulfuric acid to remove metal ion contaminants. All chemicals were used as purchased.

0.1 M sodium bicarbonate in river water was prepared as an electrolyte to further explore the ability of DDT-Au and PC-Au to catalyze CO_2R. We obtained the river water from the Olentangy river, located in Columbus, Ohio, the United States of America. Before using the river water, it was gravity filtered three times (Fisher Scientific, P4, Medium-Fine, Particle Retention: 4-8 μm).

Zn and Cu ion deposition and X-ray photoelectron spectroscopy

In order to obtain enough ion signal to detect ion deposition for x-ray photoelectron spectroscopy (XPS) analysis, we performed chronoamperometry experiments in bicarbonate and added 10 μM $ZnCl_2$ and 10 μM $Cu(NO_3)_2$. A potential of -1.1 V vs. RHE was applied for 40 min. XPS spectra were collected with a Kratos Axis Ultra x-ray photo-electron spectrometer (monochromatic Al Kα X-ray source, E_{photon} = 1486.6 eV, pass energy 20 eV).

Imaging

The images of PPh_3-Au were obtained by a JEOL 2010F transmission electron microscopy/scanning transmission electron microscopy(TEM/STEM). The images of UVO-Au were obtained by a Philips CM-200 TEM on a 50 nm Silicon Nitride film. The HAADF-STEM image was obtained on a Thermo Scientific Themis Z S/TEM at 300 kV.

ICP-MS

Semi-Quantitative measurements performed on a Perkin-Elmer ElanDRC ii Inductively Coupled Plasma Mass Spectrometer.

2. ECSA

The electrochemically active surface area is determined using the ferricyanide/ferrocyanide redox couple as shown in figure S5. We presume the reaction is site independent. By varing the scan rate we can obtain the I_p current. A plot of I_p vs. the square root of the scan rate will give a line with a slope that is proportional to the ECSA. The ECSA is determined by dividing the slope by the proportionality parameters shown in Equation 1

$$I_p = (2.69 \times 10^5) n^{3/2} A D^{1/2} C \nu^{1/2} \tag{1}$$

where I_p is the peak current (A), n=1, D is the diffusion coefficient (cm^2/s), D_o(ferri-)Fe^{3+} = 0.726 (+/-0.011) * 10^{-5}, D_R(ferrocyanide) Fe^{2+}= 0.667 (+/-0.014) * $10^{-}5$, ν is the scan rate (V/s), C is the concentration of potassium ferricyanide (mol/cm^3), 5 mM $K_3Fe(CN)_6$ and 0.1 M KCl, A is the electrode area (cm^2).

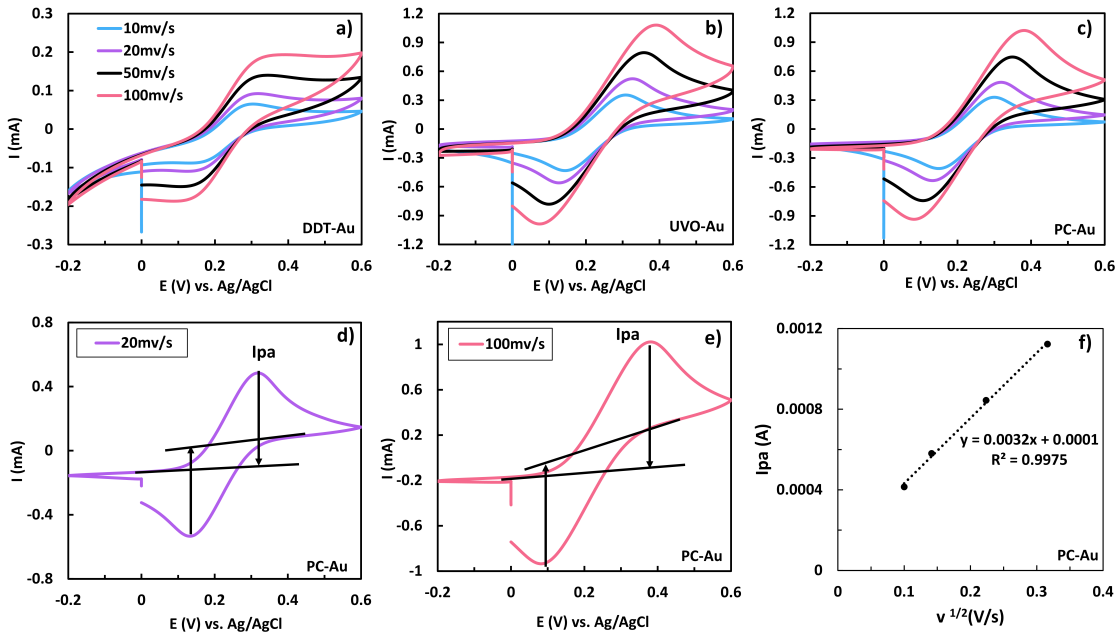

Figure S5: (a, b, c) Measured electrochemical active surface area using 5 mM $K_3Fe(CN)_6$ in 0.1 M KCl on different samples (d, e) Examples on how to define I_{pa} on PC-Au f) I_{pa} as a function of $\nu^{1/2}$ on PC-Au

3. Surface coverage calculation by XPS

Monochromatic Al Kα X-ray source (See experimental details) was used in XPS measurements at the Au 4f edge, which gives a mean free path on the order of 10 nm for these photoelectrons. It is reasonable to regard the ratio of S to Au in XPS as the ratio of S to bulk Au since these ultrasmall Au nanoparticles have a diameter of 2 nm, which is much smaller than the probe depth. To obtain the ratio of S to surface Au, we assume a truncated octahedron with a radius of 1.0 nm as given by Hostetler,[7] which gives 314 total atoms and 174 surface atoms. For example, based on our XPS results, DDT-Au shows a ratio of 0.33 for S to bulk Au, which gives a surface coverage of 0.60 for S to surface Au (0.33 x 314/174) and is in agreement with Hostetler.[7] The same calculation was also done for DDT-Au after 1 h and 2 h electrolysis, which gives a ratio of 0.20 and 0.13 for S to surface Au separately (From the S/Au of 0.11 and 0.07 by XPS).

It seems that there is some critical surface coverage of DDT that is necessary to effectively

block deposition of ions. This may be related to the ability of gauche defects to increase the volume fraction of DDT surface ligands, enabling ion blocking even when the DDT coverage decreases. During the first two hours we are above this critical surface coverage; however it appears we lose this critical surface coverage at longer times. From the S/Au ratio after 2 h of electrolysis, we can estimate this critical coverage, and find that it is ∼0.13. Future studies may show that it is possible to regenerate the catalyst with DDT post reaction or dynamically on stream.

4. Active site density calculation

Au has a crystal structure of face centered cubic. The Au(100) plane was used to calculate the active site density. There are 2 atoms per Au(100) unit cell face. The area of Au(100) is given by $8R^2$ where R is the radius of Au (0.144 nm). The active site density on Au(100) is equal to the number of atoms in plane divided by the planar area, which is 2 atoms divided by $8R^2$ giving an active site density of 1.2 x 10^{15} atoms/cm^2.

5. Stability of DDT on Au nanoparticles

Post electrolysis DDT-Au was characterized by TEM as shown in figure S6. The morphology and the size of these nanoparticles did not change significantly when compared to fresh samples indicating that the morphology of small DDT-Au nanoparticles is preserved during CO_2R. The stability of dodecanethiol was examined by both cyclic voltammetry (CV) measurements and XPS. CV measurements under different conditions on different samples were taken as shown in figure S7. To prepare PC-Au with surface-adsorbed thiol molecules, PC-Au is soaked in 2 mM thiol solution .[5] CV results show that following self-assembly of the dodecanethiol a new peak appears around -0.1 V for PC-Au with thiol molecules as shown in figure S7 (a). This peak corresponds to oxidative re-adsorption of the thiol molecules to the gold surface as has been shown previously.[5] The desorption peak is presumably also

present but is difficult to observe because this reduction peak is overlapped with catalytic wave for CO_2 reduction and hydrogen evolution. This desorption and re-adsorption process is reversible because the reduced thiol molecules have a low solubility in the electrolyte which prevents their diffusion from the electrode surface to the bulk solution. As a comparison, a CV measurement was conducted for DDT-Au from -1.9 V to 1.6 V vs. RHE as shown in figure S7 (c), this oxidative re-adsorption of thiol molecules was observed clearly. However, this feature was not clearly observed on DDT-Au from -1.3 V to 1.6 V vs. RHE. To understand what might occur to the capping agents on Au nanoparticles under electrolysis condition (-1.1 V vs. RHE), XPS measurements were conducted on fresh DDT-Au, and after 1 and 2 hours of electrolysis. A summary of the sulfur to gold ratio and ECSA are shown in table S2. These results show that 67% of the dodecanethiol ligands were lost during the first hour of electrolysis and the ECSA increased correspondingly. While only 12% of the total ligands were lost during the second hour electrolysis and ECSA increased as well. Furthermore, after 2 hour electrolysis, DDT-Au sample start to decay presumably due to the loss of the capping agents as shown in figure S8.

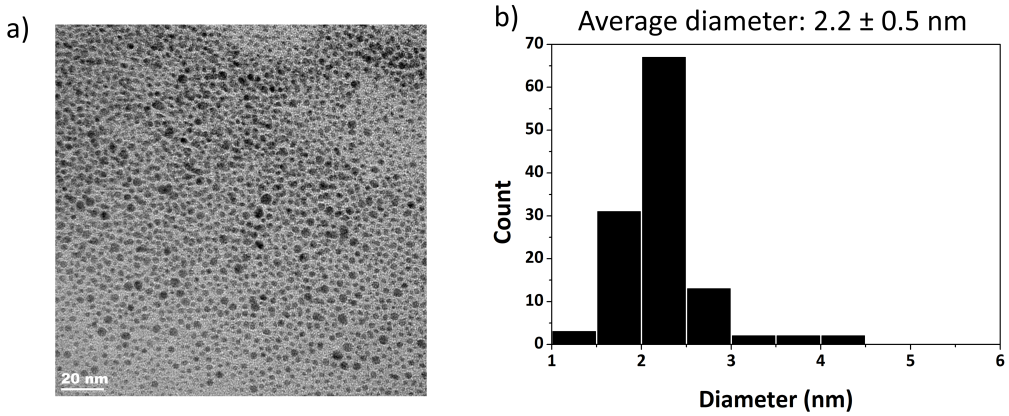

Figure S6: (a) TEM characterization and (b) histogram of 2 hour post electrolysis DDT-Au nanoparticles

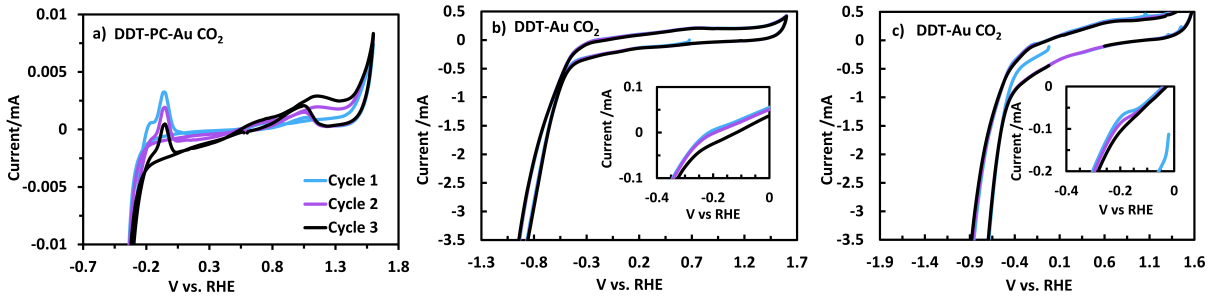

Figure S7: Cyclic measurements in 0.1 M $NaHCO_3$ on different samples a) DDT-PC-Au under CO_2 purged electrolyte from -0.7 V to 1.6 V vs. RHE. b) DDT-Au under CO_2 purged electrolyte from -1.3 V to 1.6 V vs. RHE. d) DDT-Au under CO_2 purged electrolyte from -1.9 V to 1.6 V vs. RHE

Table S2: Sulfur to gold ratio and electrochemical active surface area (ECSA) for samples at the indicated time at -1.1 V vs RHE.

Sample	Time(Hr)	S/Au	ECSA (cm^2)
DDT-Au	0	0.33	0.15
DDT-Au	1	0.11	0.55
DDT-Au	2	0.07	0.78
DDT-PC-Au	0	0.03	1.2
DDT-PC-Au	1	0	*

*not measured

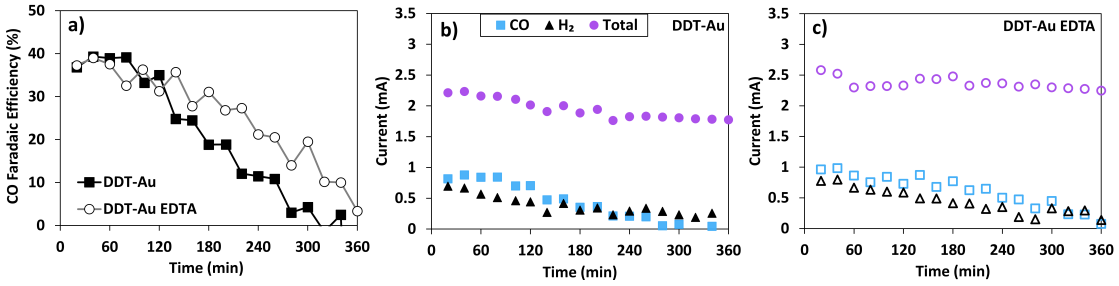

Figure S8: Faradaic efficiency to CO and partial current of each product for DDT-Au over 6 hour electrolysis in 0.1 M sodium bicarbonate electrolyte with and without 3.4 μM EDTA.

6. XPS of Cu deposition

To observe the ability of the dodecanethiol surface ligand to limit ion deposition during CO_2R, we performed CO_2R in electrolyte containing both 10 μM $Cu(NO_3)_2$ together with 10 μM $ZnCl_2$. X-ray photoelectron spectroscopy (XPS) was used to quantify both Cu and Zn on the post reaction electrodes. Results of Zn deposition are shown in Figure 1 of the main manuscript, and here we show analogous results for Cu deposition. Figure S9 shows the XPS spectrum at the Cu 2p edge for DDT-Au, PC-Au, UVO-Au. The Cu 2p peak appears as a doublet due to spin orbit coupling with Cu $2p_{1/2}$ at 952 eV and Cu $2p_{3/2}$ at 932 eV. All spectra are on the same scale for comparison. Less Cu is deposited on the DDT-Au (Cu:Au atomic ratio of 2.60) relative to PC-Au (Cu:Au atomic ratio of 13.0) and UVO-Au (Cu:Au atomic ratio of 4.95). For the Au 4f edge, Zn 3p overlapping with Au feature was observed for PC-Au and UVO-Au.

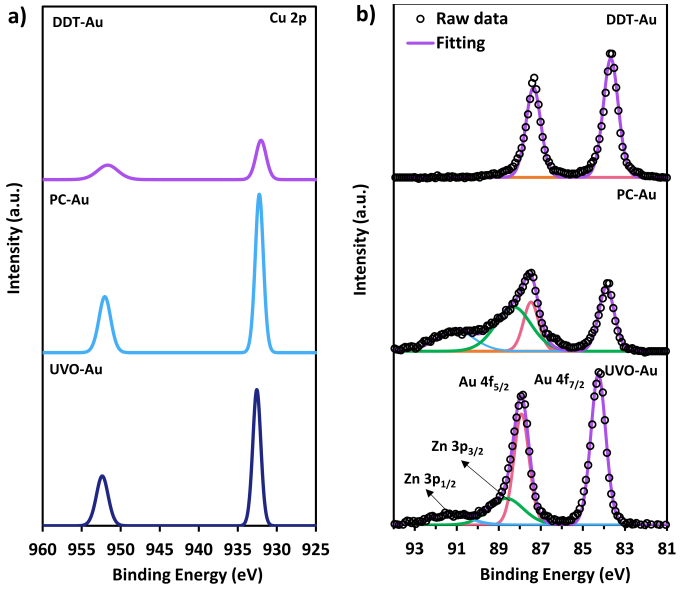

Figure S9: XPS of (a) Cu 2p (b) Au 4f on DDT-Au, PC-Au and UVO-Au following electrolysis at -1.1 V vs RHE in 0.1 M sodium bicarbonate electrolyte containing 10 μM of $Cu(NO_3)_2$. Peak integration shows that the Cu:Au atomic ratio is 2.60, 13.0, and 4.95 on DDT-Au, PC-Au, and UVO-Au, respectively.

7. DDT packing structure

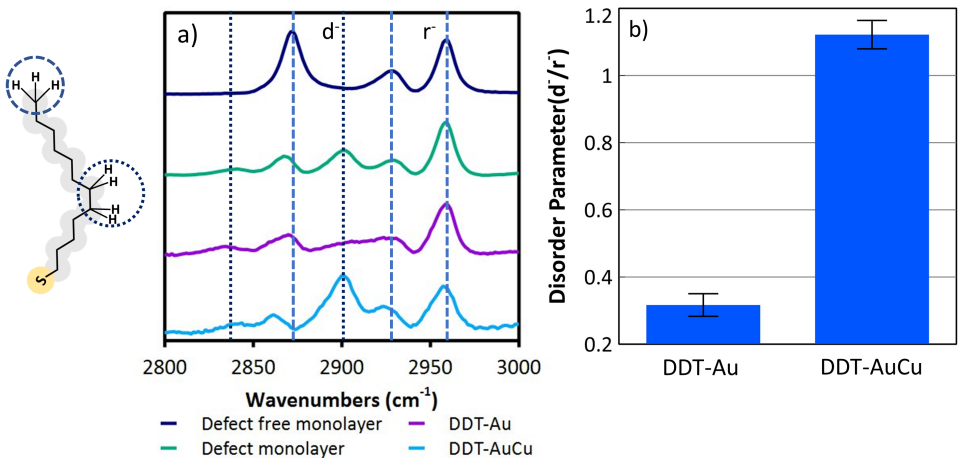

Figure S10: a) SFG spectra from a self- assembled monolayer of dodecanethiol on Au with and without gauche defects. These defects are observed as CH_2 stretches that not observed for a tightly packed monolayer b) This disorder is quantified using the ratio of the d^- and r^- bands, which we call a disorder parameter: CH_2/CH_3.

On PC-Au, dodecanethiol can form tight-packed self assembled monolayers. These well packed monolayers form almost exclusively in the all-trans configuration. However, after ageing, these chains can develop some cis bonds, called gauche defects. Figure S10 (a) shows the SFG spectra from a self-assembled monolayer of dodecanethiol on PC-Au with and without gauche defects. VSFG signal from the terminal methyl group results in three stretches, the CH_3 anti-symmetric stretch (r^-) at 2955 cm^{-1}, a fermi resonance (r^+_{FR}) between the symmetric methyl stretch and bending overtones at 2925 cm^{-1}, and a symmetric stretch (r^+) at 2868 cm^{-1}. In the presence of gauche defects, two additional stretches appear. An anti-symmetric CH_2 (d^-) stretch at 2900 cm^{-1} and a symmetric stretch (d^+) at 2840 cm^{-1} are observed.[8,9] The d^-/r^- ratio, or order parameter, can be used as a metric of the relative number of gauche defects between samples. Figure S10 (b) shows the ratio of the CH_2 anti-symetric stretch (d^-) and the CH_3 anti-symetric stretch (r^-). The magnitude of the order parameter for DDT-CuAu is much greater than that for the DDT-Au. This indicates that DDT forms a more disordered ligand shell on DDT-CuAu nanoparticles than it does on

DDT-Au. This disorder likely opens gaps in the capping agent into which ions can diffuse and deposit on the electrode.

Although these SFG spectra were obtained in air, our previous work has shown that the structure of a DDT monolayer does not show structural changes in electrolyte compared to in air.[10] This is not surprising since water is expected to be a poor solvent for dodecanethiol.

The defect free monolayer and defect monolayer were prepared by soaking electron beam films of gold in 2 mM ethanolic solutions of dodecanethiol overnight. The samples were removed and washed with ethanol. The defect monolayer was aged for a week in a clean atmosphere before measuring. Nanoparticle samples were prepared by drop casting nanoparticle 0.5 mM solutions on silicon substrates. The SFG system has been reported previously.[11] The infrared field was 3 μJ and was centered at 2918 cm^{-1}. The 800 nm field had an energy of 10 μJ. Nonresonant signal was suppressed by delaying the time-assymetric 800 nm pulse 530 fs relative to the broadband IR pulse. Spectra were integrated for 60 s.

8. CO_2R kinetics in the presence of EDTA

Figure S11 (a), (b) and (c) show the Faradaic efficiency to CO and the partial current density for PPh_3-Au. These particles exhibit a similar selectivity towards CO as the DDT-Au at early times, but the CO Faradaic efficiency decays over time. Interestingly, the current increases over time, and appears to be correlated to the loss in CO activity and the increase in H_2 activity. Figure S11 (d), (e) and (f) show the Faradaic efficiency to CO and the partial current density for DDT-CuAu. These nanoparticles show an initial CO Faradaic efficiency of 15% as expected due to a smaller number of Au sites. DDT-CuAu shows a slow decay in CO Faradaic efficency, but a stable efficiency in the presence of EDTA. This can be attributed to the order of the capping agent on these nanoparticles.

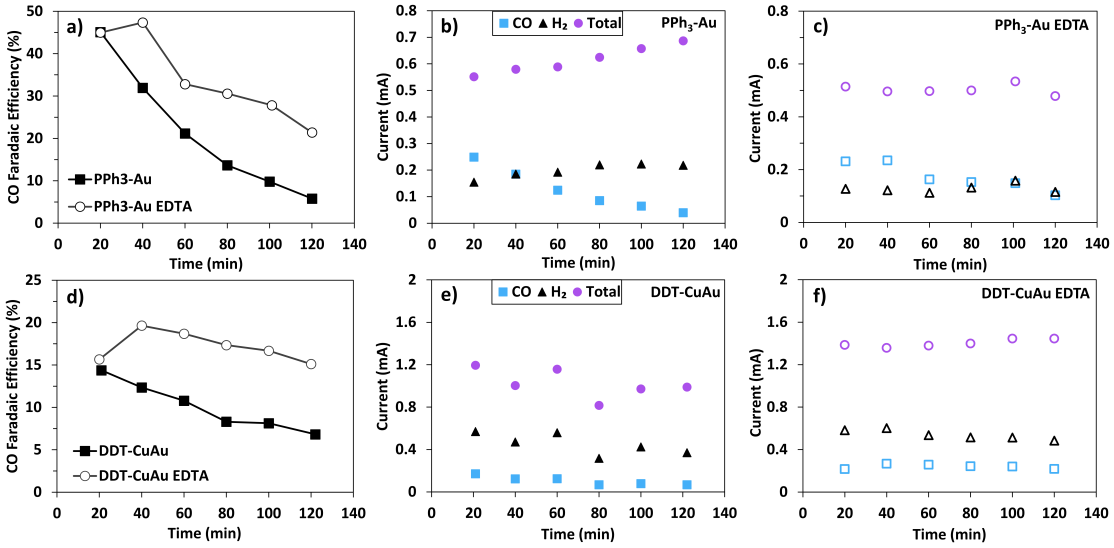

Figure S11: Faradaic efficiency to CO and partial current of each product for PPh_3-Au and DDT-CuAu

9. Identification of other products

Table S3 shows the Faradaic efficiency of all products produced on DDT-Au. The total Faradaic efficiency is less than 100%, which is due to systemic losses. To correct for these losses we ran HER in 0.5 M H_2SO_4 using Pt, which has a Faradaic efficiency of 100%. We chose a voltage which gave a similar current density to DDT-Au and PC-Au. All samples were normalized to this experiment. Methane, ethane and ethylene are detectable but the Faradaic efficiency is below 0.1 %. The formate only shows for DDT-CuAu with a Faradaic efficiency of 2 %. The low Faradaic efficiency of CO is due to the size effect of Au nanoparticles, smaller Au nanoparticles tend to show more under-coordinated site, where HER is more favored. [12]

Table S3: Faradaic efficiency of main products of different samples over 120 min

Product	DDT-Au (%)	UVO-Au (%)	PC-Au (%)	PPh_3-Au (%)	DDT-CuAu (%)
Hydrogen	40.0	32.1	63.4	49.8	68.2
Carbon monoxide	57.2	69.7	27.6	31.2	16.0
Methane	<0.1	<0.1	<0.1	<0.1	<0.1
Ethane	<0.1	<0.1	<0.1	<0.1	<0.1
Ethylene	<0.1	<0.1	<0.1	<0.1	<0.1
Formate	<0.1	<0.1	<0.1	<0.1	2

10. CO_2R kinetics in ambient water

To determine how effective the DDT-Au particles are, we obtained an ion-abundant water sample from the Olentangy river, in Columbus, Ohio. Table S4 shows the concentration for a selected number of ions in the Olentangy river, which were obtained through ICP-MS.

Using this as our water source, and after the addition of bicarbonate, we ran CO_2R on DDT-Au and PC-Au. Figure S12 shows the CO Faradaic efficiency, and partial current to each product as a function of time. As seen, the DDT-Au has a higher selectivity to CO, and loss in selectivity is also slower.

Table S4: List of ions in Olentangy river water by abundance.

Ion	Concentration (ppb)
Ca	58239
Mg	19373
Sr	550
Al	199
Ba	53
Ni	16
Fe	14
U	10
Zn	9.6
Cu	5.6
Cr	4.2
Mo	4.1
Ti	3.4
Zr	3.1
Sc	1.8
Rb	0.6
V	0.5
Sn	0.2
Sb	0.2
Co	0.2
Mn	0.1
Pb	0.1
Ga	0.1
Rh	0.1

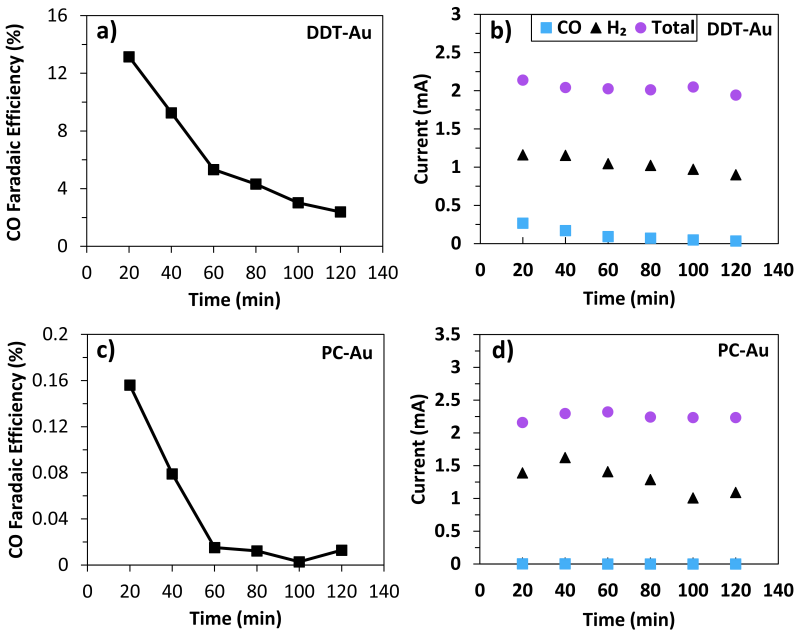

Figure S12: Faradaic efficiency to CO and partial current of each product for DDT-Au (a and b), PC-Au (c and d) using Olentangy river water source as electrolyte

References

(1) Hofmann, D. M.; Fairbrother, D. H.; Hamers, R. J.; Murphy, C. J. *ACS Appl. Nano Mater.* **2019**, *2*, 3989–3998.

(2) Brust, M.; Walker, M.; Bethell, D.; Schiffrin, D. J.; Whyman, R. *J. Chem. Soc., Chem. Commun.* **1994**, 801–802.

(3) Chen, S.; Sommers, J. M. *J. Phys. Chem. B* **2001**, *105*, 8816–8820.

(4) Aliaga, C.; Park, J. Y.; Yamada, Y.; Lee, H. S.; Tsung, C.-K.; Yang, P.; Somorjai, G. A. *J. Phys. Chem. C* **2009**, *113*, 6150–6155.

(5) Yang, D.-F.; Wilde, C.; Morin, M. *Langmuir* **1997**, *13*, 243–249.

(6) Wuttig, A.; Surendranath, Y. *ACS Catal.* **2015**, *5*, 4479–4484.

(7) Hostetler, M. J.; Wingate, J. E.; Zhong, C.-J.; Harris, J. E.; Vachet, R. W.; Clark, M. R.;

Londono, J. D.; Green, S. J.; Stokes, J. J.; Wignall, G. D. et al. *Langmuir* **1998**, *14*, 17–30.

(8) Bordenyuk, A. N.; Weeraman, C.; Yatawara, A.; Jayathilake, H. D.; Stiopkin, I.; Liu, Y.; Benderskii, A. V. *J. Phys. Chem. C* **2007**, *111*, 8925–8933.

(9) Lambert, A. G.; Davies, P. B.; Neivandt, D. J. *Appl. Spectrosc. Rev.* **2005**, *40*, 103–145.

(10) Wallentine, S.; Bandaranayake, S.; Biswas, S.; Baker, L. R. *J. Phys. Chem. A* **2020**, *124*, 8057–8064.

(11) Biswas, S.; Wallentine, S.; Bandaranayake, S.; Baker, L. R. *J. Chem. Phys.* **2019**, *151*, 104701.

(12) Mistry, H.; Reske, R.; Zeng, Z.; Zhao, Z.-J.; Greeley, J.; Strasser, P.; Cuenya, B. R. *J. Am. Chem. Soc.* **2014**, *136*, 16473–16476.